Journal of Sustainability Science and Management
Volume 18 Number 12, December 2023: 28-42
eISSN: 2672-7226

EFFECT OF THE INCORPORATION OF CHOLINE CHLORIDE-BASED DEEP EUTECTIC SOLVENT ON THE FLEXIBILITY OF POLY(METHYL METHACRYLATE) FILMS

FAMIZA ABDUL LATIF[1], NABILAH AKEMAL MUHD ZAILANI[2]*, KHUZAIMAH NAZIR[2], RIZANA YUSOF[2], FAZNI SUSILA ABDUL GHANI[1], MOHD AZLAN MOHD ISHAK[2] AND SHARIL FADLI MOHD ZAMRI[1]

[1]Faculty of Applied Sciences, Universiti Teknologi MARA, Selangor Branch, Puncak Alam Campus, 42300 Puncak Alam, Selangor, Malaysia. [2]Faculty of Applied Sciences, Universiti Teknologi MARA, Perlis Branch, Arau Campus, 02600 Arau, Perlis, Malaysia.

**Corresponding author: nabilahakemal@uitm.edu.my*
Submitted final draft: 4 February 2023 *Accepted: 5 June 2023* http://doi.org/10.46754/jssm.2023.12.004

Abstract: The addition of ionic liquid (IL) during the free-radical polymerisation of methyl methacrylate (MMA) led to the successful production of a flexible PMMA film. In this study, a more affordable and less hazardous Deep Eutectic Solvent (DES), made up of choline chloride and 1,4-butanediol in a 1:3 mole ratio, was utilised as a substitute for IL. Interestingly, the incorporation of 50 wt.% of DES ($PMMA_{DES50}$) produced a flexible film which was confirmed by the decrease in the glass transition temperature (T_g). The increase in ionic conductivity up to 2.56 x 10^{-8} S cm^{-1} was also observed for $PMMA_{DES50}$. The enhancement in the amorphous phase of the sample was achieved by minimising the hydrogen bond of PMMA, which was made possible by the large structure of DES occupying the space between the polymer chains. The Fourier Transform Infrared (FTIR) analysis confirmed the existence of interaction between PMMA and DES, leading to the observed improvement in the thermal stability of the $PMMA_{DES}$ system. The incorporation of 10 wt.% of lithium triflate (LiTf) into the $PMMA_{DES50}$ tremendously increased the ionic conductivity to 2.56 × 10^{-6} S cm^{-1}. This proved that $PMMA_{DES50}$ serves as a good and novel polymer host which provides an amorphous phase that eases the movement of lithium ions.

Keywords: Deep Eutectic Solvent, PMMA, polymerisation, polymer electrolyte, flexible film.

Introduction

The latest technologies require high-density energy storage materials (i.e., batteries, supercapacitors, and fuel cells) that are safe and flexible to power various types of electrical devices (Koohi-Fayegh & Rosen, 2020). Liquid electrolytes (LE) are widely used in commercial energy storage devices due to their high ionic conductivity. However, the use of LE is not environmentally friendly as it is susceptible to leakage, corrosion, and even explosion. One of the safest types of electrolytes in the energy storage system is solid-based polymer electrolytes. Among the polymer-based electrolyte systems studied, poly(methyl methacrylate) (PMMA) was found to be the most mechanically stable electrolyte concerning the electrode (Zhou *et al.,* 2020). However, this can only be achieved if the PMMA electrolyte is prepared in the form of a thin film. Unfortunately, commercially available PMMA films were brittle due to their polar nature and tended to crosslink via hydrogen bonds between chains.

Several modifications were made to overcome the brittleness of the PMMA films, such as by adding plasticisers (Guan *et al.,* 2020), fillers (Li *et al.,* 2020) or blending with another polymer (Tamiya *et al.,* 2020). Unfortunately, these modifications did not fully satisfy the property of a workable electrolyte. Previously, the flexible, conducting, and free-standing films of PMMA electrolytes had been successfully obtained by incorporating a large structure of ionic liquid (IL) such as 1-methyl-3-pentamethyl disiloxymethylimidazolium bis(trifluoromethyl sulfonyl)imide (Zailani *et al.,* 2017), N-propyl-

methyl piperidinium bis(trifluoromethyl sulfonyl) imide (Libo *et al.,* 2014) and 1-butyl-1-methylpiperidinium chloride/1-butyl-1-methyl piperidinium bis(trifluoromethyl sulfonyl)imide (Wu *et al.,* 2019) during free radical polymerisation of MMA. This success is contributed by the inhibition of the hydrogen bonding as the large structure of IL occupied the space between PMMA chains during the polymerisation process. Unfortunately, ILs are expensive (del Monte *et al.,* 2014) and require complicated preparation techniques. Therefore, in this study, a cheaper and less toxic deep eutectic solvent (DES) with similar properties to IL was used for the polymerisation of PMMA.

DES consists of a hydrogen bond acceptor (HBA) and hydrogen bond donor (HBD) which can self-associate to form a new eutectic mixture at a melting point lower than the melting point of each constituent (Tomé *et al.,* 2018). At this eutectic point, the mixture of DES will remain in the homogenous liquid phase (Shafie *et al.,* 2019). There are four (4) types of DES which differ based on their composition including Type I (quaternary ammonium salt + metal chloride), Type II (quaternary ammonium salt + metal chloride hydrate), Type III (quaternary ammonium salt + hydrogen bond donor) and Type IV (metal chloride hydrate + hydrogen bond donor). According to Shafie *et al.* (2019), Type III DES requires low-cost preparation and presents low eco-toxicity. Therefore, in this study, Type III DES consisting of choline chloride (ChCl):1,4 butanediol (1,4-BD) (σ = 0.92 mS cm^{-1}) was selected. In addition, ChCl-polyol DES is known to be miscible in the acrylic system (Mota-Morales *et al.,* 2018). In this study, the ChCl:1,4-BD DES (1:3 mole ratio) was synthesised using a well-established direct heating method (Othman *et al.,* 2015) as it is not commercially available.

To date, there were only a few studies which had reported on the synthesis of a new type of polymer electrolytes via free radical polymerisation in DES for application in energy storage devices (Mukesh *et al.,* 2016; Qin & Panzer, 2017). However, the studies concentrated on the fabrication of gel electrolytes which were shown to suffer from mechanical instability after a few cycles. Thus, in this study, only solid PMMA containing DES ($PMMA_{DES}$) was fabricated into films using the solvent casting technique. The structural, morphological, electrical, and thermal properties of the $PMMA_{DES}$ system were determined by Fourier Transform Infrared Spectroscopy (FTIR), Optical Microscope (OM), Electrochemical Impedance Spectroscopy (EIS), Differential Scanning Calorimetry (DSC) and Thermogravimetric Analysis (TGA) respectively. Valuable insights have been gained from the results obtained, shedding light on the role of DES in the creation of flexible PMMA electrolyte films. Furthermore, the use of biodegradable DES in this research has the potential to promote a more eco-friendly environment. By introducing varying amounts of lithium triflate (LiTf) to the most conductive sample in the $PMMA_{DES}$ system, lithium ions mobility was examined. The EIS method was employed to determine the ionic conductivity of the LiTf-doped $PMMA_{DES}$ system. To the best of our knowledge, this particular investigation had not yet been conducted.

Materials and Methods

Synthesis of DES

The synthesis of DES via the direct heating method was adapted from the study of Othman et al. (2015). Firstly, ChCl: 99% (Acros Organic) and 1,4-BD: > 99% (Sigma) with a mole ratio of 1:3 were mixed. Then, the mixture was stirred and heated at 80°C on the hotplate until dissolution and appearance of a clear viscous solution.

Synthesis of $PMMA_{DES}$

For the synthesis of $PMMA_{DES}$, 2.00 g of MMA (Sigma) monomer was mixed with 5 wt.% of benzoyl peroxide (BPO) (Sigma) as the initiator. Then, the solution was stirred and heated in the shaking water bath at 80°C until solidification. The steps were repeated with the addition of 10, 30 and 50 wt.% of DES into the solution of

MMA and BPO (Ramesh *et al.,* 2012; Hamsan *et al.,* 2020). The sample designation, along with the composition of $PMMA_{DES,}$ is listed in Table 1. The addition of DES beyond 50 wt.% was not carried out as this study focuses on PMMA as the main material.

Preparation of $PMMA_{DES}$ Films

In this study, only solid $PMMA_{DES}$ were fabricated into films using the solvent casting technique. For the preparation of $PMMA_{DES}$ films, 0.5 g of the solid $PMMA_{DES0}$ was dissolved in 20 mL of tetrahydrofuran (THF) (Sigma). The dissolved PMMA solution was placed in a Teflon dish and kept in the fume hood until the formation of the film. Next, the film was peeled off from the Teflon dish and kept in the oven at 40°C for a few hours. The film was then kept in the desiccator before further characterisation. The steps were repeated using $PMMA_{DES10}$, $PMMA_{DES30}$ and $PMMA_{DES50}$. For the formation of LiTf-doped $PMMA_{DES}$ films, the steps were repeated by the addition of 5 wt.%, 10 wt.% and 15 wt.% of LiTf into the $PMMA_{DES}$ sample with the highest ionic conductivity (Naiwi *et al.,* 2022; Khan *et al.,* 2022).

Fourier Transform Infrared Spectroscopy

Fourier Transform Infrared Spectroscopy (FTIR) (Thermo Fisher Scientific Nicolet iS10 Spectrometer) equipped with Attenuated Total Reflectance (ATR) was used to confirm the structure of DES and complete polymerisation of PMMA. It was also used to determine the interaction between PMMA and DES. The spectra were recorded in the wavenumber range of 4000-600 cm^{-1} and a resolution of 2 cm^{-1} by using the transmittance mode.

Optical Microscope

An optical microscope (Nikon ECLIPSE ME 600) was used to observe the morphology of the $PMMA_{DES}$ films. The sample was placed on a microscope slide and the image was captured at 10x magnification.

Electrochemical Impedance Spectroscopy

The electrochemical impedance spectroscopy (EIS) (HIOKI 3532-50 LCR Hi Tester analyser) was used to obtain the impedance of the film samples. The film sample was sandwiched between two stainless steel electrodes with a diameter of 0.6 cm. Then, the impedance measurements were carried out within the frequency range of 100 Hz to 1 MHz at ambient temperature. The bulk resistance (R_b) of the sample was determined from the impedance plots obtained and the ionic conductivity (σ) of the samples was calculated using Equation (1).

$$\sigma = \frac{l}{R_b \cdot A} \quad (1)$$

where R_b is the bulk resistance (Ω), l denotes the thickness of the film (cm) and A represents the effective contact area of the electrode and the electrolyte (cm^2).

Differential Scanning Calorimetry

Differential Scanning Calorimetry (DSC) analysis was carried out using DSC TA Q2000. The $PMMA_{DES}$ films weighing about 10 mg were crimped in standard aluminium pans, while a crimped empty aluminium pan was used as the reference cell. Tzero Press was used to crimp the lids and pans close together to improve thermal contact between the sample, the pan, and the

Table 1: Sample designation and composition of $PMMA_{DES}$

Sample Designations	Mass of MMA (g)	Mass of DES (g)	Percentage of DES (wt.%)	Weight of BPO (g)
$PMMA_{DES0}$	2.00	0.00	0	0.10
$PMMA_{DES10}$		0.21	10	
$PMMA_{DES30}$		0.80	30	
$PMMA_{DES50}$		1.87	50	

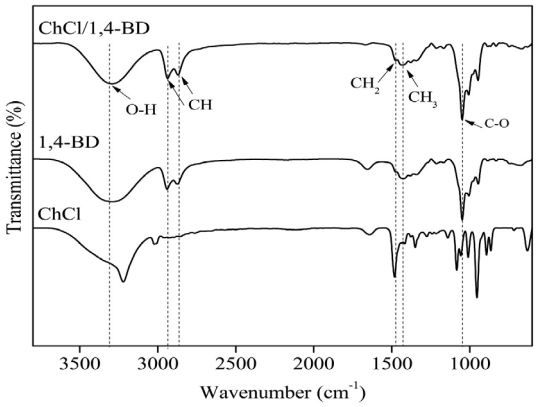

(a)

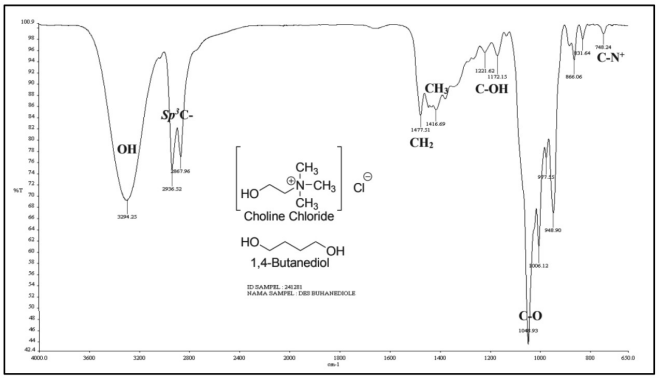

(b)

Figure 1: (a) FTIR spectra of ChCl, 1,4-BD and ChCl/1,4-BD (this study) and (b) FTIR spectrum of ChCl/1,4-BD (Othman *et al.,* 2015)

disc during measurements as well as reduce spillage. Then, the samples were heated from 20°C to 120°C at a heating rate of 10°C min^{-1} under dry nitrogen gas (flow rate: 50 mL min^{-1}).

Thermogravimetric Analysis

Thermogravimetric Analysis (TGA) was conducted using a thermogravimetric analyser (Pyris 1 Perkin Elmer). 3 mg of the $PMMA_{DES}$ films were placed into an aluminium pan. The samples were then heated from room temperature to 500°C at a heating rate of 10°C min^{-1} in the nitrogen atmosphere.

Results and Discussion

Synthesis of DES

The homogenous liquid mixture was successfully obtained for ChCl/1,4-BD. The mixture was observed to remain in liquid condition even at room temperature. Figure 1 (a) shows the FTIR spectra for pure ChCl, pure 1,4-BD and ChCl/1,4-BD while Figure 1 (b) depicts the FTIR spectrum of the previously synthesised ChCl/1,4-BD along with its structure.

It was observed that the FTIR spectrum for ChCl/1,4-BD showed peaks at 3291 cm^{-1}, 2936 cm^{-1} and 2869 cm^{-1}, 1484 cm^{-1}, 1421 cm^{-1} and 1045 cm^{-1} representing OH stretching, C-H

stretching, CH_2 bending, CH_3 bending and C-O stretching, respectively. All the observed FTIR peaks matched well with the previous study on the ChCl/1,4-BD (Othman *et al.,* 2015) [Figure 1 (b)]. It was observed that the O-H stretching peak of ChCl/1,4-BD at 3291 cm^{-1} experienced downshifting of the wavenumber and reduced peak intensity if compared to pure 1,4-BD. This observation confirmed the hydrogen bonding interactions between ChCl and 1,4-BD as illustrated in Figure 2.

Synthesis of $PMMA_{DES}$

A series of solid $PMMA_{DES0}$ – $PMMA_{DES50}$ (Figure 3) was successfully obtained after the free radical polymerisation of MMA in DES for 35 minutes.

Formation of $PMMA_{DES}$ Films

Brittle films were observed for $PMMA_{DES0}$ and $PMMA_{DES10}$ samples. Solid, flexible, and free-standing films can only be obtained when > 30 wt.% of DES was incorporated into the PMMA matrix during free radical polymerisation (Figure 4).

Conductivity studies of the $PMMA_{DES}$ System

Figure 5 depicts the Nyquist plots for $PMMA_{DES0}$-$PMMA_{DES50}$ at room temperature. All plots exhibited tilted spikes at high-frequency regions which denoted the capacitance characteristics of the samples (Zailani *et al.,* 2017).

$PMMA_{DES0}$ exhibited an ionic conductivity of 1.42 x 10^{-8} S cm^{-1}. When 10 wt.% of DES was added, the ionic conductivity decreased to 1.01 x 10^{-8} S $cm^{-1,}$ suggesting the conglomeration of DES particles, which restricted the mobility of chloride ions as shown in Figure 6.

The ionic conductivity was then observed to increase with the addition of 30 and 50 wt.% of DES to 1.93 x 10^{-8} S cm^{-1} and 2.56 × 10^{-8} S cm^{-1}, respectively. It is possible that

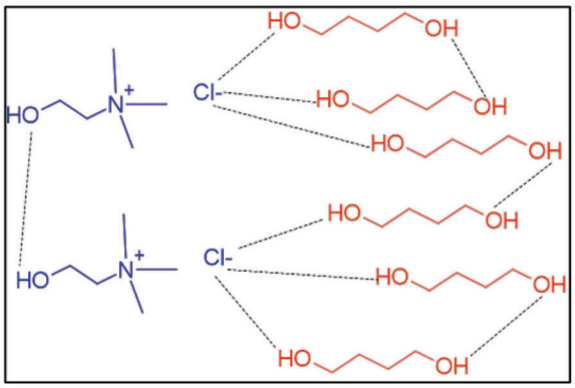

Figure 2: Possible hydrogen bonding interactions in 1:3 mole ratio of ChCl/1,4-BD

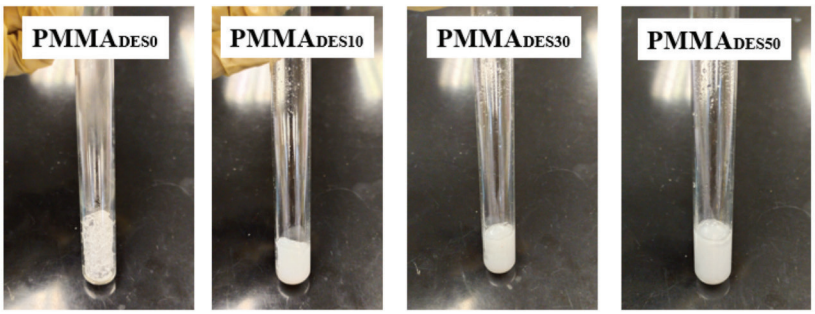

Figure 3: The photographs of solid $PMMA_{DES}$ system

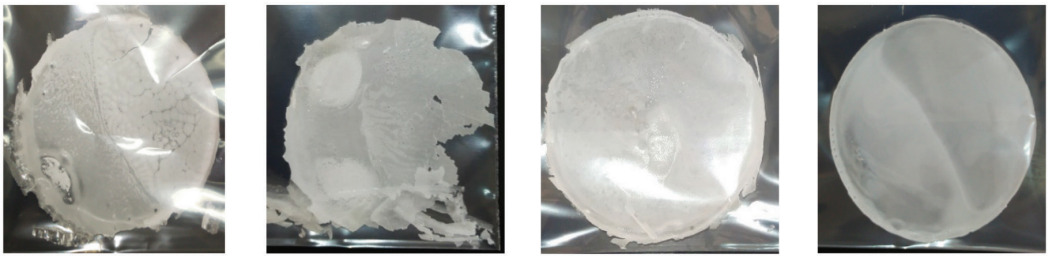

(a) (b) (c) (d)

Figure 4: The photographs of (a) $PMMA_{DES0}$, (b) $PMMA_{DES10}$, (c) $PMMA_{DES30}$ and (d) $PMMA_{DES50}$ films

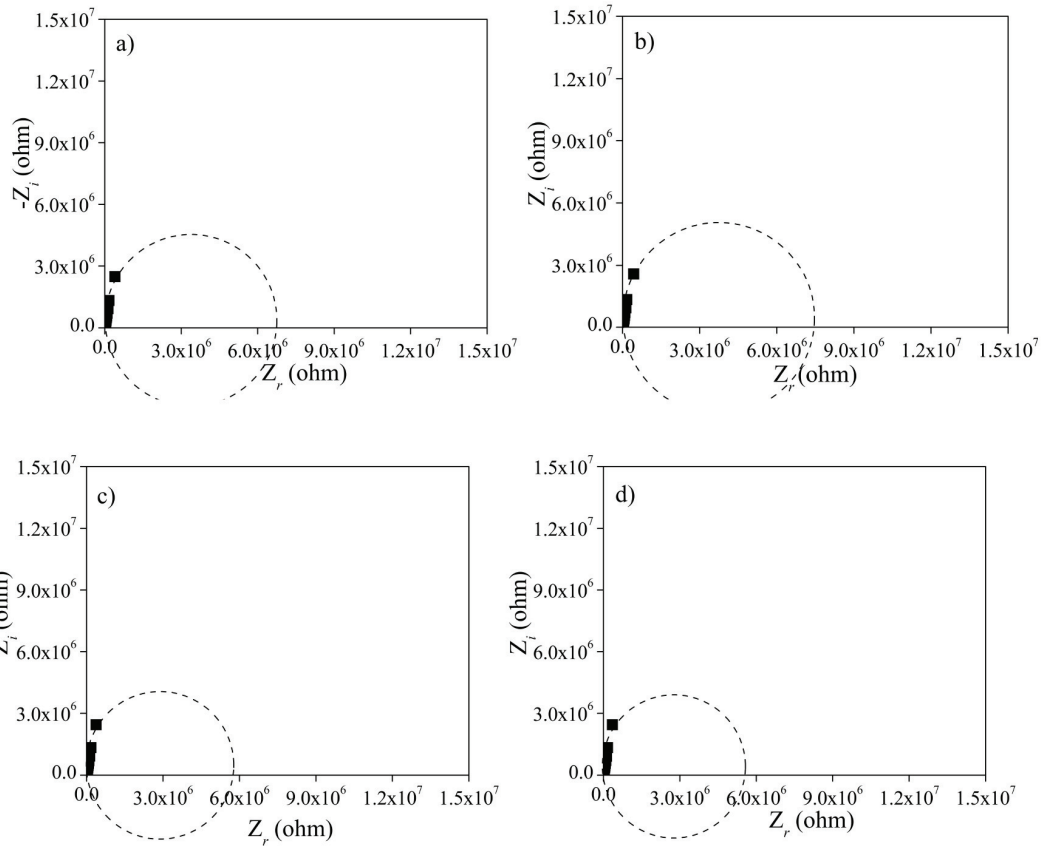

Figure 5: Nyquist plots for (a) $PMMA_{DES0}$, (b) $PMMA_{DES10}$, (c) $PMMA_{DES30}$ and (d) $PMMA_{DES50}$

the observed phenomenon is attributable to the reduction of hydrogen bonding within the PMMA matrix. This can be explained by the successful encapsulation of a large DES structure, which occupies the space between the chains as depicted in Figure 7.

This contributed to the availability of more amorphous areas which can facilitate the mobility of chloride ions, thereby improving the ionic conductivity of the samples. A similar observation had also been reported by Ramesh and their co-workers (2012) on the study of doped ethylene glycol/urea-corn starch polymer electrolytes. Table 2 lists the ionic conductivity of the other polymer electrolyte systems synthesised via free radical polymerisation techniques. The ionic conductivity of these

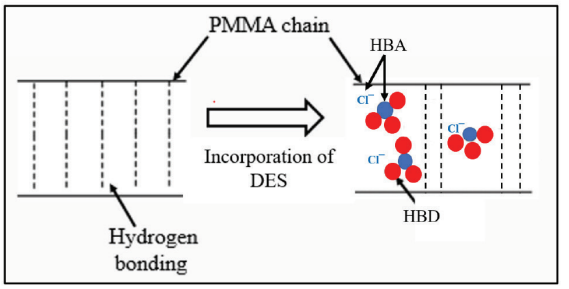

Figure 6: Conglomeration of DES particles in $PMMA_{DES10}$

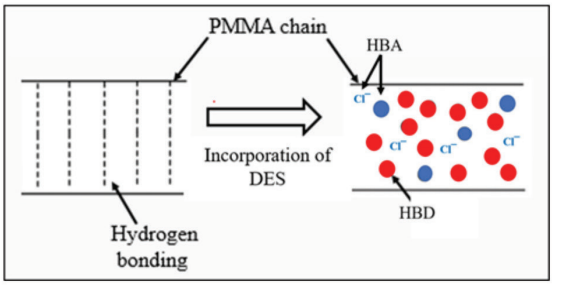

Figure 7: Disruption of hydrogen bonding in $PMMA_{DES30}$ and $PMMA_{DES50}$

Table 2: The ionic conductivity of the other polymer electrolyte systems

System	Percentage of DES (vol. %)	Type	Ionic Conductivity (S cm^{-1})	References
Poly acrylic acid (PAA)/Choline chloride-Glycerol	83.0	Gel	3.33×10^{-3}	Yang *et al.* (2022)
Poly (2-hydroxyethyl methacrylate) (PHEMA)-co-poly(ethylene glycol) diacrylate (PEGDA)/Choline chloride-Glycerol	86.8	Gel	5.70×10^{-3}	Qin and Panzer (2022)

systems was significantly higher than ours. However, the samples were in the gel form which was shown to suffer from mechanical instability after a few cycles.

OM Studies of the $PMMA_{DES}$ System

Figure 8 depicts the optical micrographs for the $PMMA_{DES}$ system. Figure 8 (a) shows the morphology for pure PMMA film that displayed a granule-like structure with random orientation. It was observed that there were more grains available in PMMA film if compared to other samples, hence explaining its brittle structure. The micrographs for $PMMA_{DES10}$ showed a congested structure which might be due to the conglomeration of DES particles. This observation was also reported by Ramesh and his co-workers (2012) when above 20 wt.% DES was added to the corn starch. Meanwhile, the increase in grain size was observed to occur for $PMMA_{DES30}$ and $PMMA_{DES50}$ [Figures 8 (c) and 8 (d)], signifying the successful encapsulation of DES between PMMA chains. This observation was also reported in the study of PMMA/ $[(SiOSi)C_1C_1im][NTf_2]$ done by Zailani *et al.* (2017). The enlargement of grains caused a

merging effect between neighbouring grains, which subsequently led to a decrease in the number of grains. This reduction in the number of grains was observed to contribute to the increase in the amorphous phase of the samples, as depicted in Figure 8 (d). Furthermore, the addition of 50 wt.% of DES was observed to increase the ionic conductivity, as confirmed by EIS analysis.

FTIR Studies of the $PMMA_{DES}$ System

Figure 9 shows the FTIR spectra for DES and $PMMA_{DES}$ systems, while Table 3 lists the wavenumber of the characteristic peaks.

It was found that the characteristic peaks for PMMA appeared in the FTIR spectrum of $PMMA_{DES0}$ at 2950 cm^{-1}, 1442 cm^{-1}, 1238 cm^{-1} and 1725 $cm^{-1,}$ contributing to C-H stretching, $C\text{-}H_2$ bending, C-O-C stretching and C=O stretching, respectively. Aside from that, the C=C stretching (~1640 cm^{-1}) (Tommasini *et al.,* 2018) peak associated with MMA also disappeared from the FTIR spectrum of $PMMA_{DES0}$. This confirms that the polymerisation of PMMA had been successfully carried out via free radical polymerisation.

When DES was incorporated during the free radical polymerisation of PMMA, new peaks representing DES were detected at ~3300 cm^{-1} and ~1050 cm^{-1} which denoted O-H stretching and C-N stretching, respectively. This indicates that the DES has been successfully incorporated into the PMMA matrix. As a consequence, the upshift of the C-O-C stretching peak of PMMA was observed to occur from 1238 cm^{-1} for $PMMA_{DES0}$ to 1242 cm^{-1} for $PMMA_{DES50}$. The changes in the peak intensities for both C-O-C and C=O stretching peaks were also observed, hence confirming the interaction that occurred between oxygen atoms of PMMA with the choline cation and hydrogen atom of DES, as illustrated in Figure 10.

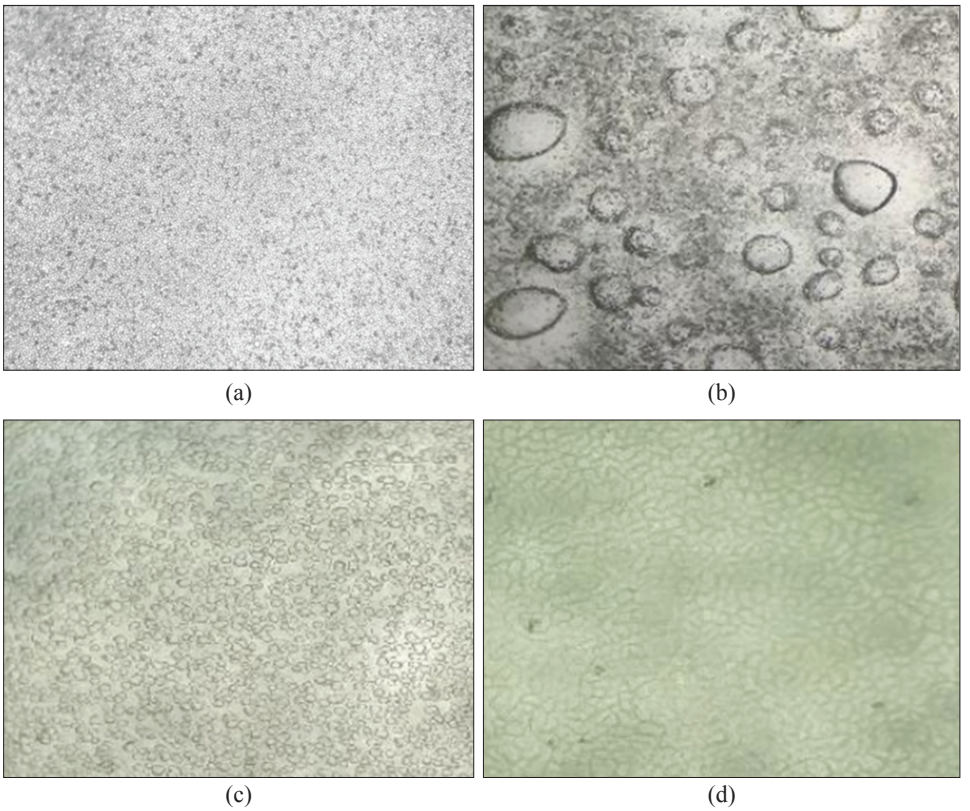

(a) (b)

(c) (d)

Figure 8: OM micrographs for (a) $PMMA_{DES0}$, (b) $PMMA_{DES10}$, (c) $PMMA_{DES30}$ and (d) $PMMA_{DES50}$

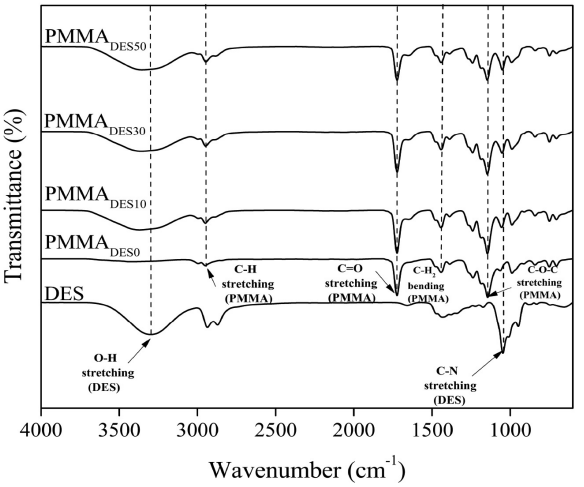

Figure 9: FTIR spectra for DES and PMMA$_{DES}$ system

Table 3: Characteristic peaks of DES and PMMA$_{DES}$ system

Peaks	Wavenumbers (cm^{-1})					
	DES	PMMA$_{DES0}$	PMMA$_{DES10}$	PMMA$_{DES30}$	PMMA$_{DES50}$	References
C=O stretching	-	1724	1723	1723	1723	Zailani *et al.* (2017)
C-O-C stretching	-	1238	1241	1242	1242	Prasad & Lal (2022)
CH_2 bending	1431	1442	1444	1443	1443	Prasad & Lal (2022)
C-H stretching	-	2950	2950	2948	2948	Prasad & Lal (2022)
OH stretching	3302	3445	3368	3362	3353	Shafie *et al.* (2019)
C-N stretching	1047	-	1055	1053	1051	Shafie *et al.* (2019)

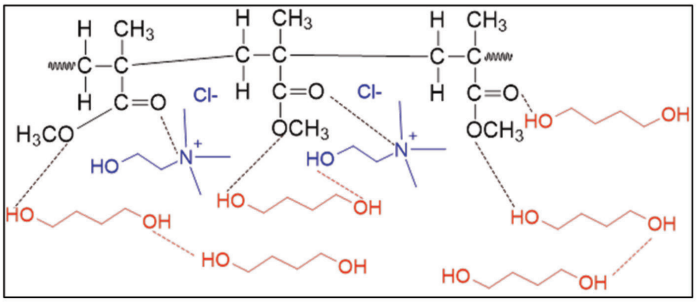

Figure 10: Possible interactions between PMMA and DES

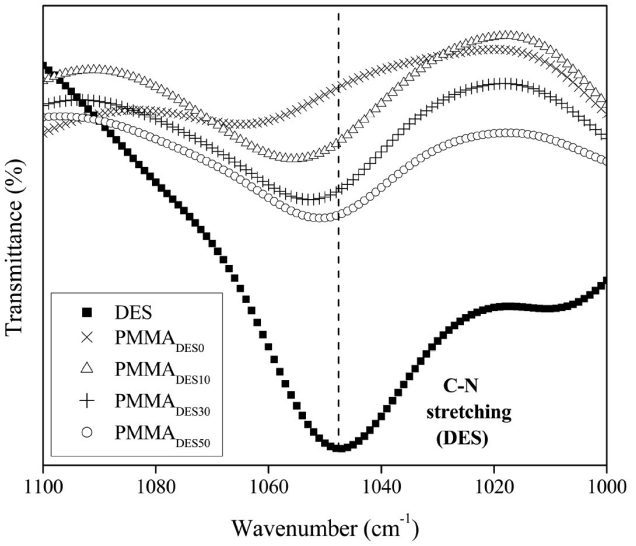

Figure 11: C-N stretching peaks for PMMA$_{DES}$ system

This can be further supported by the change in the peak intensities of C-N stretching and O-H stretching of DES (Figure 9). The highest intensity of C-N stretching of DES was observed for the PMMA$_{DES50}$ sample as shown in Figure 11 which indicates the presence of the highest amount of charges. This can be further supported by the reduced grain numbers as shown in OM

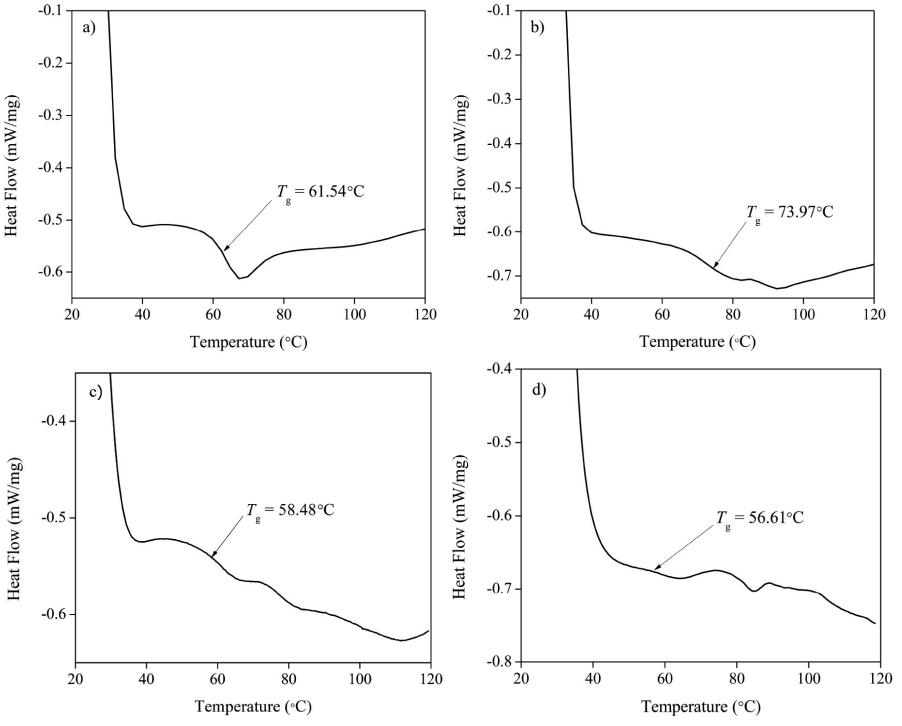

Figure 12: DSC thermograms for (a) PMMA$_{DES0}$, (b) PMMA$_{DES10}$, (c) PMMA$_{DES30}$ and (d) PMMA$_{DES50}$

analyses [Figure 8 (d)] as well as an increase in the ionic conductivity with the addition of 50 wt.% of DES.

DSC Studies of the $PMMA_{DES}$ System

Figure 12 shows the DSC thermograms for the $PMMA_{DES}$ system. The glass transition temperature (T_g) for $PMMA_{DES0}$ film obtained in this study was 61.54°C. This value was in good agreement with the results reported by a previous study (Mohammadi *et al.,* 2018).

The value of T_g increased upon the addition of 10 wt.% of DES and this was due to the conglomeration of DES particles which restricted the chain flexibility. The T_g gradually decreased with the addition of 30 and 50 wt.% of DES. The lowest value of T_g (56.61°C) for sample $PMMA_{DES50}$ indicated its highest chain mobility. This proves that the incorporation of 50 wt.% DES had successfully hindered the formation of hydrogen bonding between the polar polymer chains of PMMA hence increasing the chain flexibility. The disruption of hydrogen bonding in PMMA resulted in the alteration of its semicrystalline structure, leading to the formation of a more amorphous phase. This increase in the amorphous phase subsequently facilitated polymer segmental mobility within the polymer chain, thereby enabling $PMMA_{DES50}$ to attain its highest ionic conductivity value. The T_g obtained for this $PMMA_{DES}$ system was slightly better than the one obtained in the PMMA-$BMIPF_6$ system (Jiang *et al.,* 2006).

TGA Studies of the $PMMA_{DES}$ System

Figure 13 depicts the TGA thermograms for the $PMMA_{DES}$ system. The previous study showed that PMMA prepared by free radical polymerisation displayed three-stage decomposition temperatures (Gao *et al.,* 2001). The same observation was also obtained in this study as the TGA thermogram for $PMMA_{DES0}$ exhibited three steps of thermal decomposition (T_d) at 117°C, 246°C, and 320°C. The first stage is characterised by the decomposition of weak head-to-head linkages and the release of impurities previously trapped in the PMMA. In the second stage, the degradation is attributed to the breakdown of the side chain of PMMA. Finally, in the third stage, the main chain of PMMA goes through decomposition.

Interestingly, the degradation temperatures observed for the side chain and main chain of $PMMA_{DES10}$-$PMMA_{DES50}$ were higher than that of $PMMA_{DES0}$ which suggested that the incarcerated DES significantly increased the thermal stability of the newly synthesised $PMMA_{DES10}$-$PMMA_{DES50}$. This was due to the interaction that occurred between oxygen atoms

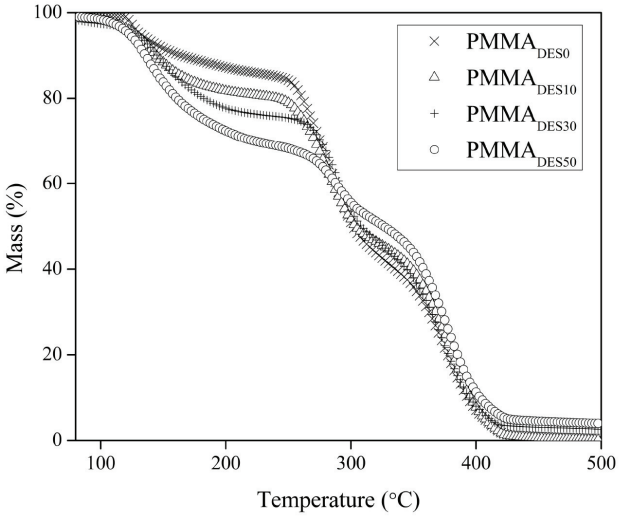

Figure 13: TGA thermogram for $PMMA_{DES}$ system

of PMMA with the choline cation of ChCl and hydrogen atom of 1,4-BD as confirmed from the FTIR analysis.

Formation of LiTf Doped $PMMA_{DES}$ Films

The highest conducting sample in the $PMMA_{DES}$ system, $PMMA_{DES50}$ was doped with different percentages of LiTf. Figure 14 shows the photographs of LiTf-doped $PMMA_{DES}$ films. Upon addition of 5 wt.% of LiTf into the $PMMA_{DES}$ system [Figure 14 (a)], a half-flexible and half-brittle solid film was observed. Meanwhile, solid, flexible, and free-standing film was observed with the incorporation of 10 wt.% LiTf [Figure 14 (b)]. The incorporation of LiTf at 15 wt.% resulted in a film that displayed brittleness [Figure 14 (c)]. The EIS measurement was carried out only on the PMMADES films that were doped with 5 and 10 wt.% LiTf.

Conductivity Studies of the LiTf Doped $PMMA_{DES}$ Films

Figure 15 illustrates the Nyquist plots for $PMMA_{DES50}$/5% LiTf and $PMMA_{DES50}$/10% LiTf at room temperature. Both plots exhibited half semicircle at a high-frequency region which denoted the ion migration in the bulk system (Zailani *et al.,* 2017). The appearance of a spike at lower frequencies region in the Nyquist plot of $PMMA_{DES50}$/10% LiTf was due to the capacitance characteristic of the samples (Deraman *et al.,* 2014).

The values of R_b were obtained from the intercept of the spike with the extrapolation of the semi-circular region on the Z_r axis. Then, the ionic conductivities for LiTf doped $PMMA_{DES}$ system were calculated based on Equation (1). The conductivity was observed to increase to 1.07×10^{-7} S cm^{-1} and 2.56×10^{-6} S cm^{-1} when

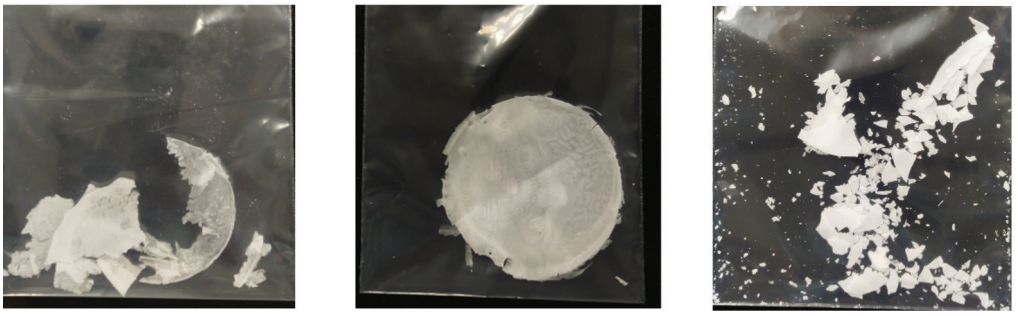

(a) (b) (c)

Figure 14: The Photographs of (a) $PMMA_{DES50}$/5% LiTf, (b) $PMMA_{DES50}$/10% LiTf and (c) $PMMA_{DES50}$/15% LiTf

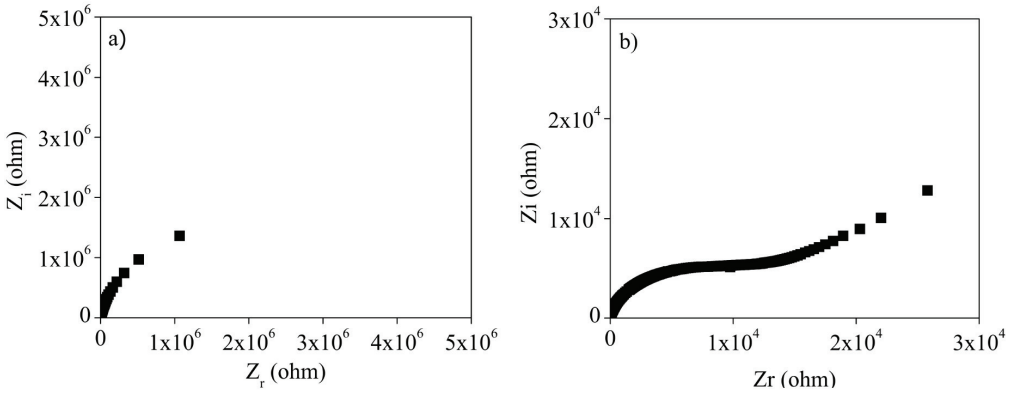

Figure 15: Nyquist plots for (a) $PMMA_{DES50}$/5% LiTf and (b) $PMMA_{DES50}$/10% LiTf

5 and 10 wt.% LiTf were added, respectively. The increase in the conductivity indicated that $PMMA_{DES50}$ serves as a good and novel polymer host which provides an amorphous phase that can ease the movement of lithium ions. Thus, $PMMA_{DES50}$ has the potential to be used as electrolytes in energy storage devices as the doping of other additional conducting species might produce higher ionic conductivity.

Conclusion

A novel series of solid $PMMA_{DES}$ were successfully synthesised when 10, 30 and 50 wt.% of DES were incorporated during the free radical polymerisation of MMA. Interestingly, the incorporation of 50 wt.% of DES ($PMMA_{DES50}$) during free radical polymerisation of MMA produced the flexible film with improved ionic conductivity of 2.56×10^{-8} S cm^{-1}. This was due to the improvement in the amorphous phase of the sample contributed by the breakage of the hydrogen bond of PMMA as the large structure of DES occupied the space between the polymer chains. This was supported by the reduction in the number of grains for $PMMA_{DES50}$ as observed in OM analysis. The decrease in the glass transition temperature (T_g) of $PMMA_{DES50}$ to 56.61°C hence, further confirmed the increase in the chain flexibility of the film. The FTIR analysis proved the occurrence of interaction between PMMA and DES and due to that, the improvement in the thermal stability of the $PMMA_{DES}$ system was observed in the TGA analysis. The incorporation of 10 wt.% of LiTf tremendously increased the ionic conductivity to 2.56×10^{-6} S cm^{-1}, hence, proving the ability of $PMMA_{DES50}$ to provide the amorphous phase that can ease the movement of lithium ions.

Acknowledgements

The authors thank the Faculty of Applied Sciences, UiTM Perlis branch for giving their full support for this research. Financial support by MyRA Lepasan PhD grant (600-RMC/GPM LPHD 5/3 (084/2022)) is highly acknowledged.

References

del Monte, F., Carriazo, D., Serrano, M. C., Gutiérrez, M. C., & Ferrer, M. L. (2014). Deep eutectic solvents in polymerizations: A greener alternative to conventional syntheses. *ChemSusChem, 7*(4), 999-1009.

Deraman, S. K., Mohamed, N. S., & Subban, R. H. Y. (2014). Ionic liquid incorporated PVC-based polymer electrolytes: Electrical and dielectric properties. *Sains Malaysiana*, *43*, 877-883.

Gao, Z., Xie, W., Hwu, J., Wells, L., & Pan, W. P. (2001). The characterization of organically modified montmorillonite and its filled PMMA nanocomposite. *Journal of Thermal Analysis and Calorimetry*, *64*(2), 467-475.

Guan, S., Wang, W., Zheng, J., & Xu, C. (2020). A method to achieve full incorporation of PMMA-based gel electrolyte in fibre-structured PVB for solid-state electrochromic device fabrication. *Electrochimica Acta, 354*, 136702.

Hamsan, M. H., Aziz, S. B., Nofal, M. M., Brza, M. A., Abdulwahid, R. T., Hadi, J. M., & Kadir, M. F. Z. (2020). Characteristics of EDLC device fabricated from plasticized chitosan: $MgCl_2$ based polymer electrolyte. *Journal of Materials Research and Technology*, *9*(5), 10635-10646.

Jiang, J., Gao, D., Li, Z., & Su, G. (2006). Gel polymer electrolytes are prepared by in situ polymerization of vinyl monomers in room-temperature ionic liquids. *Reactive and Functional Polymers*, *66*(10), 1141-1148.

Khan, N. M., & Samsudin, A. S. (2022). Electrical conduction of PMMA/PLA doped lithium bis (oxalate) borate-based hybrid gel polymer electrolyte. *Materials Today: Proceedings*, *51*, 1460-1464.

Koohi-Fayegh, S., & Rosen, M. A. (2020). A review of energy storage types, applications and recent developments. *Journal of Energy Storage, 27*, 101047.

Li, J., Hu, R., Zhou, H., Tao, S., & Wang, Y. (2020). Nano-SiO_2@ PMMA-doped

composite polymer PVDF-HFP/PMMA/PEO electrolyte for lithium metal batteries. *Journal of Materials Science: Materials in Electronics, 31*(3), 2708-2719.

Libo, L., Jiesi, L., Shuo, Y., Shaowen, G., & Peixia, Y. (2014). Gel polymer electrolytes containing ionic liquids prepared by radical polymerization. *Colloids and Surfaces A: Physicochemical and Engineering Aspects, 459*, 136-141.

Mohammadi, M., Davoodi, J., Javanbakht, M., & Rezaei, H. (2018). Glass transition temperature of PMMA/modified alumina nanocomposite: Molecular dynamic study. *Materials Research Express*, *6*(3), 035309.

Mota-Morales, J. D., Sánchez-Leija, R. J., Carranza, A., Pojman, J. A., del Monte, F., & Luna-Bárcenas, G. (2018). Free-radical polymerizations of and in deep eutectic solvents: Green synthesis of functional materials. *Progress in Polymer Science, 78*, 139-153.

Mukesh, C., Upadhyay, K. K., Devkar, R. V., Chudasama, N. A., Raol, G. G., & Prasad, K. (2016). Preparation of a Noncytotoxic Hemocompatible Ion Gel by self-polymerization of HEMA in a green deep eutectic solvent. *Macromolecular Chemistry and Physics*, *217*(17), 1899-1906.

Naiwi, T. S. R. T., Aung, M. M., Rayung, M., Ahmad, A., Chai, K. L., Fui, M. L. W., ... & Aziz, N. A. A. (2022). Dielectric and ionic transport properties of bio-based polyurethane acrylate solid polymer electrolyte for application in electrochemical devices. *Polymer Testing*, *106*, 107459.

Othman, Z. S., Hassan, N. H., & Zubairi, S. I. (2015). Alcohol-based-deep eutectic solvent (DES) as an alternative green additive to increase rotenone yield. *AIP Conference Proceedings, 1678*(1), 050004.

Prasad, S. G., & Lal, C. (2022). Spectroscopic investigations of optical bandgap and search for reaction mechanism chemistry due to γ-Rays irradiated PMMA polymer. *Biointerface Research in Applied Chemistry*, *13*, 1-18.

Qin, H., & Panzer, M. J. (2017). Chemically cross-linked poly (2-hydroxyethyl methacrylate)-supported deep eutectic solvent gel electrolytes for eco-friendly supercapacitors. *ChemElectroChem*, *4*(10), 2556-2562.

Ramesh, S., Shanti, R., & Morris, E. (2012). Studies on the plasticization efficiency of deep eutectic solvent in suppressing the crystallinity of corn starch-based polymer electrolytes. *Carbohydrate polymers*, *87*(1), 701-706.

Ramesh, S., Shanti, R., & Morris, E. (2012). Studies on the plasticization efficiency of deep eutectic solvent in suppressing the crystallinity of corn starch-based polymer electrolytes. *Carbohydrate Polymers*, *87*(1), 701-706.

Shafie, M. H., Yusof, R., & Gan, C. Y. (2019). Synthesis of citric acid monohydrate-choline chloride-based Deep Eutectic Solvents (DES) and characterization of their physicochemical properties. *Journal of Molecular Liquids*, *288*, 111081.

Tamiya, T., Cui, X., Hsu, Y. I., Kanno, T., Asoh, T. A., & Uyama, H. (2020). Enhancement of interfacial adhesion in immiscible polymer blend by using a graft copolymer synthesized from propargyl-terminated poly (3-hydroxybutyrate-co-3-hydroxy hexanoate). *European Polymer Journal, 130*, 109662.

Tomé, L. I., Baião, V., da Silva, W., & Brett, C. M. (2018). Deep eutectic solvents for the production and application of new materials. *Applied Materials Today*, *10*, 30-50.

Tommasini, F. J., Ferreira, L. D. C., Tienne, L. G. P., Aguiar, V. D. O., Silva, M. H. P. D., Rocha, L. F. D. M., & Marques, M. D. F. V. (2018). Poly (methyl methacrylate)-SiC

nanocomposites prepared through in situ polymerization. *Materials Research*, *21*(6), e20180086. https://doi.org/10.1590/1980-5373-MR-2018-0086

Wu, L., Chen, Z., & Ma, X. (2019). Chloride ion conducting polymer electrolytes based on cross-linked PMMA-PP_{14}Cl-PP_{14}TFSI ion gels for chloride ion batteries. *International Journal of Electrochemical Science, 14*, 2414-2421. http://www.electrochemsci.org/papers/vol14/140302414.pdf

Yang, H., Sang, M., Li, G., Zuo, D., Xu, J., & Zhang, H. (2022). Stretchable, self-healable, conductive and adhesive gel polymer electrolytes based on a deep eutectic solvent for all-climate flexible electrical double-layer capacitors. *Journal of Energy Storage*, *45*, 103766.

Zailani, N. A. M., Latif, F. A., Ali, A. M. M., Zainuddin, L. W., Kamaruddin, R., & Yahya, M. Z. A. (2017). Effect of ionic liquid incarceration during free radical polymerization of PMMA on its structural and electrical properties. *Ionics, 23*(2), 295-301.

Zhou, Z., Feng, Y., Wang, J., Liang, B., Li, Y., Song, Z., & Song, J. (2020). A robust, highly stretchable ion-conducive skin for stable lithium metal batteries. *Chemical Engineering Journal, 396*, 125254.